



RESEARCH ARTICLE OPEN ACCESS

Supraspinal Plasticity of Axonal Projections From the Motor Cortex After Spinal Cord Injury in Macaques

Satoko Ueno^{1,2}  | Reona Yamaguchi^{1,2}  | Kaoru Isa¹  | Toshinari Kawasaki^{1,3} | Masahiro Mitsuhashi^{1,4}  | Kenta Kobayashi^{5,6}  | Jun Takahashi⁷  | Tadashi Isa^{1,2,8} 

¹Department of Neuroscience, Graduate School of Medicine, Kyoto University, Kyoto, Japan | ²Institute for the Advanced Study of Human Biology (WPI-ASHBi), Kyoto University, Kyoto, Japan | ³Department of Neurosurgery, Graduate School of Medicine, Kyoto University, Kyoto, Japan | ⁴Department of Neurology, Graduate School of Medicine, Kyoto University, Kyoto, Japan | ⁵Section of Viral Vector Development, National Institute for Physiological Sciences, Okazaki, Japan | ⁶Department of Physiological Sciences, School of Life Science, The Graduate University for Advanced Studies (SOKENDAI), Hayama, Japan | ⁷Department of Clinical Application, Center for iPS Cell Research and Application, Kyoto University, Kyoto, Japan | ⁸Human Brain Research Center, Graduate School of Medicine, Kyoto University, Kyoto, Japan

Correspondence: Tadashi Isa (isa.tadashi.7u@kyoto-u.ac.jp)

Received: 2 September 2024 | **Revised:** 17 November 2024 | **Accepted:** 25 November 2024

Funding: This work was supported by a Grant-in-Aid for Scientific Research on Innovative Areas “Hyper-adaptability” (Project no. 19H05723), a Grant-in-Aid for Scientific Research from the Ministry of Education, Culture, Sports, Science, and Technology (MEXT) (KAKENHI (A) no. 19H01011 and (S) no. 22H04992), Japan Agency for Medical Research and Development (JP18dm0307005 to T.I.), and a Grant-in-Aid for Research Activity Start-up (Project no. 22K21240).

Keywords: hand function | lateral reticular nucleus | macaque | motor cortex | pontine nucleus | putamen | spinal cord injury

ABSTRACT

During recovery following spinal cord injury in the macaque, the sensorimotor cortex on the same side as the injury (ipsilesional, unaffected) becomes activated and plays a role in guiding movements of the affected hand. Effective regulation of these movements by the ipsilesional sensorimotor cortex would depend not only on its ability to send motor commands directly to target muscles but also on coordinated functioning with higher-level motor planning systems such as the cortico-basal ganglia and cortico-cerebellar loops. In this study, using anterograde viral tracers, we analyzed the axonal trajectories of corticofugal fibers from the contralesional (affected) primary motor cortex (M1) at the brainstem level in two macaque monkeys with sub-hemisection spinal cord injury at the mid-cervical level. They showed considerable recovery of grasping movements after injury. We found an increase in axonal projections from the contralesional M1 to the contralateral putamen, ipsilateral lateral reticular nucleus, and contralateral pontine nucleus compared to projections from the ipsilesional (unaffected) M1. We propose that these increased projections from the contralesional M1 to the striatum and precerebellar nuclei on the nondominant side may function to recruit the ipsilesional M1 through the cortico-basal ganglia and cortico-cerebellar loops to control hand movements on the affected side during recovery.

1 | Introduction

Understanding the mechanisms underlying the restoration of motor function through rehabilitative training after brain or spinal cord injury is crucial for the development of better neurorehabilitation and neuromodulation therapies. For this purpose, studies using nonhuman primate models are necessary

because the structure and function of their motor systems and physical constitution are much closer to humans than those of rodents (Courtine et al. 2007; Darian-Smith 2007; Lemon 2008; Alstermark and Isa 2012). Previously, we showed that rehabilitative training leads to the recovery of dexterous hand movements within several weeks after spinal cord injury, which includes a lesion of the lateral corticospinal tract, in macaque

This is an open access article under the terms of the [Creative Commons Attribution-NonCommercial-NoDerivs](https://creativecommons.org/licenses/by-nc-nd/4.0/) License, which permits use and distribution in any medium, provided the original work is properly cited, the use is non-commercial and no modifications or adaptations are made.

© 2024 The Author(s). The *Journal of Comparative Neurology* published by Wiley Periodicals LLC.

monkeys (Sasaki et al. 2004; Sugiyama et al. 2013). There, the ipsilesional motor cortices were found to be critical for this recovery (Nishimura et al. 2007; Chao et al. 2019), presumably through the brainstem-mediated indirect pathway to ipsilesional hand motoneurons, which has been shown in cats (Jankowska et al. 2006).

How could the ipsilesional motor cortices be activated and contribute to motor recovery? Here, we propose that the movement-related activity of the contralesional motor cortices is transmitted to the ipsilesional motor cortices through the direct callosal pathway and the subcortical pathway through the thalamus (Guillery and Sherman 2002). We recently showed the role of the callosal pathway (Mitsuhashi et al. 2024). In this study, we focus on the possible subcortical route from the contralesional primary motor cortex (M1) to ipsilesional M1 through the cortico-basal ganglia or cortico-cerebellar loops (Alexander, DeLong, and Strick 1986; Nambu 2008; Gao et al. 2018). We thought about this because, for the proper control of movements, it would be necessary for the motor cortex to recruit higher-level motor planning systems, such as the cortico-basal ganglia and cortico-cerebellar loops, in addition to sending the descending motor commands to the target muscles.

To obtain the neuroanatomical evidence explaining how the contralesional M1 became able to activate the ipsilesional M1 during recovery, we injected highly sensitive anterograde viral tracers into both the contralesional and ipsilesional M1 in a macaque model of cervical sub-hemisection spinal cord injury. In these animals, intensive behavioral training was conducted as neurorehabilitation, along with extensive electrostimulation of the motor cortex. We observed the early recovery of their coarse hand movements, enhanced activation of the ipsilesional motor cortex, and massive reorganization of corticospinal fibers (Yamaguchi et al. 2023). In addition, we compared the axonal projections from the M1 on both sides to subcortical structures such as the putamen, lateral reticular nucleus (LRN), and pontine nucleus. We found that the projections from the contralesional (affected) M1 to the nondominant side were increased compared to those from the ipsilesional (unaffected) M1. These results suggest the possibility that the affected M1 might have contributed to the activation of the unaffected M1 through the cortico-basal ganglia and/or the cortico-cerebellar loops in addition to the direct callosal pathway.

2 | Materials and Methods

2.1 | Animals

The data were obtained from the two macaque monkeys described in another article (Yamaguchi et al. 2023). They (*Macaca fuscata*, Monkey M [5 years old, male, body weight 6.0 kg], Monkey H [5 years old, male, body weight 5.7 kg]) were obtained from the National Bio-resource Project of MEXT and used in this study. All experimental procedures were performed in accordance with the National Institutes of Health Guidelines for the Care and Use of Laboratory Animals and the guidelines set forth by the Ministry of Education, Culture, Sports, Science, and Technology of Japan and were approved by the Committee

for Animal Experimentation at the Graduate School of Medicine in Kyoto University, Japan.

2.2 | Behavioral Paradigm

Before lesions, the monkeys were trained to perform a reach-and-grasp task with their right (the side to be lesioned) hand. Briefly, the monkeys were seated in a monkey chair and required to reach for and pick up a piece of sweet potato (6-mm cube) presented through or not through a vertical slit (width 9 mm). The position of the food piece was constant, and the left hand was restrained to prevent its use during the task. The behavioral task was performed in 100 trials per day for 5 months after injury, and the success rate of task performance was calculated. The monkeys were unable to perform the precision grip (a movement to pick up the food piece using the pads of the index finger and thumb) as the same as before lesioning. However, the success rate in coarse hand movements (a pinch guided by the edge of the slit or a power grip with non-fractionated finger movements) recovered in several weeks after injury.

2.3 | Surgery

All surgical procedures were performed under general anesthesia. The monkeys were first anesthetized with ketamine (10 mg/kg, IM injection) and xylazine (1 mg/kg, IM), and anesthesia was maintained with isoflurane (1%–1.5%) inhalation during surgery. Vital functions, that is, heart rate, electrocardiography, peripheral capillary oxygen saturation, PCO₂, and body temperature, were monitored throughout surgery. The monkeys were also administered Ringer's solution (30 mL/h, IV drip) continuously during surgery, and dexamethasone (0.825 mg/kg, IM), diclofenac (12.5 mg, anally), and ampicillin sodium (40 mg/kg, IM) after surgery.

2.4 | Spinal Cord Injury

A sub-hemisection of the cervical spinal cord was made between the C4 and C5 segments on the right side (Figure 1a). Under anesthesia, the spinal cord was exposed from the dorsal side through a laminectomy, and the lateral funiculus and a part of the ventral and dorsal funiculi were lesioned using a surgical blade, needle, and tweezers. The opened dura was closed using artificial dura mater. The skin and muscles were sutured with nylon or silk.

2.5 | Cortical Stimulation and Behavioral Observation

Before spinal cord injury, the monkeys were implanted with platinum electrocorticography electrodes covering the premotor cortex, M1, and somatosensory cortex of each hemisphere. Eighteen and 28 electrocorticography channels were implanted on each hemisphere of Monkeys M and H, respectively. Once a week, electrical stimuli (3 pulses at 3 mA, 0.5-ms duration, 50-ms interval) were applied every 2 s through a stimulator (Nihon Kohden, Tokyo, Japan). This train stimulation was repeated 100 times for each of the 18 channels selected from the electrocorticography

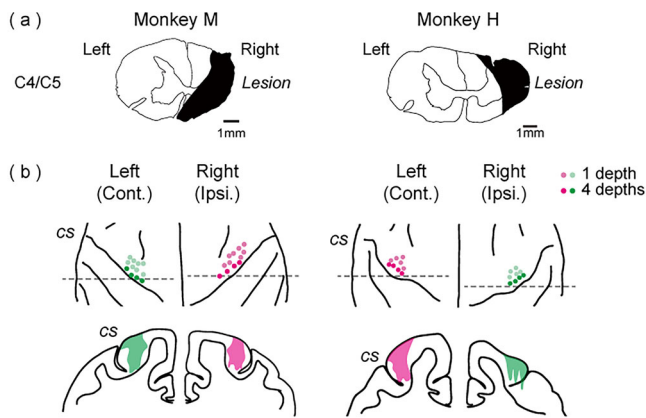


FIGURE 1 | (a) Lesion area of the spinal cord (C4/C5). (b) Injection sites of the viral tracers. Each dot indicates one track for glass needle insertion. Light colored dots indicate an injection with one depth (1.5 mm from the brain surface). Darker colored dots indicate an injection with four depths (1.5, 3.0, 4.5, and 6.0 mm from the brain surface). The bottom illustrations of the represented sections (on the dotted line in the upper illustrations) indicate the extent of viral tracers observed by direct fluorescence. cont., contralesional; CS, central sulcus; ipsi., ipsilesional.

array on both hemispheres during the observation period to test the muscle twitches of the right (lesion side) forelimb.

The recovery of hand movements was assessed as the success rate in the reach-and-grasp task. Neither monkey recovered precision grip movements after spinal cord injury. The success rates of both pinch-aided by slit and gross power grip movements became zero after spinal cord injury but increased to approximately 100% within 40 days after lesioning.

2.6 | Injection of Neural Tracers

After the behavioral observation period, two different adeno-associated viral (AAV) vectors, AAV DJ-CAGGS-EGFP or AAV DJ-CAGGS-DsRed2, were injected into the M1 of each hemisphere using a glass pipette (outside diameter at the tip was 60–110 μm) attached to a Hamilton syringe (10 μL , Model 701N, 26sG, 2 in, point style 2; Hamilton Company, Reno, NV, USA) (Figure 1b) under general anesthesia (the same protocols as described in Section 2.3).

The AAV vectors were prepared as described previously (Sano et al. 2020). Briefly, the packaging (pAAV-DJ and pHelper) and transfer plasmids (pAAV-CAGGS-EGFP and pAAV-CAGGS-DsRed2) were transfected into HEK293T cells.

In Monkey M, 24 injections of AAV DJ-CAGGS-EGFP (titer, 1.5×10^{13} vg/mL) were made at 12 tracks in the left M1 (contralesional side) on the 204th postlesion day, and 24 injections of AAV DJ-CAGGS-DsRed2 (titer, 1.2×10^{13} vg/mL) were made at 12 tracks in the right M1 (ipsilesional side) on the 211th postlesion day. In Monkey H, 21 injections for each of AAV DJ-CAGGS-DsRed2 (titer, 1.6×10^{13} vg/mL, left, contralesional side) on the 204th postlesion day and AAV DJ-CAGGS-EGFP (titer, 2.4×10^{13} vg/mL, right, ipsilesional side) were made at nine tracks on the 210th postlesion day. After inserting the glass pipette into the target

position, it was not moved for 2–5 min before injecting 0.5 μL over 5 min, and the pipette was left in position for 5 min before removing it.

2.7 | Histology

At 7 weeks after the last injection, the monkeys were deeply anesthetized and transcardially perfused with 0.05 M phosphate-buffered saline (PBS), followed by 4% paraformaldehyde in 0.1 M phosphate buffer. The brain and spinal cord were removed and immersed in sucrose following post-fixation. Coronal sections of the brain (40- μm thick), including the injection area and brainstem, were prepared using a freezing microtome (REM-710; Yamato Kohki Industrial, Saitama, Japan).

For immunohistochemistry of vector-transfected neurons, primary antibodies against GFP (RRID: AB_221569) and DsRed2 (RFP, RRID: AB_2209751) were used with subsequent enhancement through diaminobenzidine staining. All steps were performed at room temperature unless otherwise indicated. For reactions with an anti-GFP antibody, free-floating sections were quenched by 30-min incubation in 0.6% H_2O_2 in methanol after washing in 0.05 M PBS. After washing with PBS, the sections were blocked in 5% skim milk in PBS with 0.6% Triton X-100 (PBS-T) for 60 min. For reactions with an anti-RFP antibody, a blocking step was performed with 10% normal goat serum (NGS; S-1000, RRID: AB_2336615; Vector Laboratories, Burlingame, CA, USA) in PBS-T. Then, the sections were incubated with a rabbit anti-GFP antibody (1:4000, A11122, RRID: AB_221569; Invitrogen, Carlsbad, CA, USA) in PBS-T or rabbit anti-RFP antibody (1:2000, 600-401-379, RRID: AB_2209751; Rockland Immunochemicals, Inc., Boyertown, PA, USA) in 2% NGS/PBS-T overnight at 4°C. After four washes with PBS-T for 5 min each, the sections were incubated with a biotinylated goat anti-rabbit IgG antibody (1:200, BA-1000, RRID: AB_2313606; Vector Laboratories) for 2 h. After washing with PBS-T, the sections were treated with PBS-T containing avidin–biotin peroxidase complex (ABC Elite, 1:100, PK-6100, RRID: AB_2336819; Vector Laboratories) for 60 min. The sections were washed three times for 5 min each in PBS and Tris-buffered saline (TBS) and treated with TBS containing 0.04% diaminobenzidine (040-27001; FUJIFILM Wako Pure Chemical Corporation, Tokyo, Japan), 0.04% nickel chloride (147-01042; FUJIFILM Wako Pure Chemical Corporation), and 0.0003% H_2O_2 until a sufficient reaction was provided. Then, the sections were washed three times in TBS and three times in PBS for 5 min each. After being mounted on gelatin-coated glass slides, the sections were counterstained with 0.1% neutral red. Digital images were acquired using a BZ-X710 Keyence microscope.

2.8 | Data Analysis

On the stained sections of the forebrain, pons, and medulla, the putamen, pontine nucleus, and LRN were respectively analyzed using ImageJ software (Fiji; National Institutes of Health, Bethesda, MD, USA; RRID: SCR_003070). RGB images were split, and only the red channel images were used for analysis to reduce the effect of counterstaining. The areas of signals above the threshold were calculated using the Auto Threshold method in ImageJ software, and the detected areas were carefully confirmed

TABLE 1 | Summary of the percentage of pixels with signal intensity above the threshold, and the ratios of normally nondominant projection against normally dominant projections in each animal and each injection. From M1, the ipsilateral projections dominate the contralateral projections in cases of the putamen and pontine nucleus. In contrast, the contralateral projections dominate for the LRN. The data of putamen correspond to Figure 2g–j, LRN to Figure 3k–n, and pontine nucleus to Figure 4g–j.

		Contralesional (affected) side	Ipsilesional (unaffected) side		Contralesional (affected) side	Ipsilesional (unaffected) side	
M1		Left	Right Injected side	Normally Nondominant /Dominant	Left Injected side	Right	Normally Nondominant /Dominant
Putamen	Monkey M	12.1%	52.9%	0.23	55.3%	29.5%	0.53
	Monkey H	10.5%	41.8%	0.25	43.6%	17.6%	0.41
		Normally Nondominant	Normally Dominant		Normally Dominant	Normally Nondominant	
LRN	Monkey M	3.26%	1.05%	0.41	52.0%	32.1%	1.75
	Monkey H	8.75%	1.97%	0.26	4.82%	7.36%	0.68
		Normally Dominant	Normally Nondominant		Normally Nondominant	Normally Dominant	
Pontine nucleus	Monkey M	1.56%	43.2%	0.036	68.3%	21.4%	0.31
	Monkey H	0.51%	8.48%	0.061	16.1%	3.61%	0.23
		Normally Nondominant	Normally Dominant		Normally Dominant	Normally Nondominant	

by visual inspection. Data of each region of interest, defined based on anatomical structures, were then compared between the left and right sides in each section. Differences were assessed for statistical significance using paired Student's *t*-tests within sections and unpaired *t*-tests between sections.

3 | Results

The essence of the quantitative data in the results is shown in Table 1.

3.1 | Projections From the Motor Cortex to the Putamen

The projections from the ipsilesional (right; unaffected) M1 to the putamen of Monkey M are shown in Figure 2a. The contralateral projections (from right M1 to left putamen; Figure 2c) were less dense than the ipsilateral projections (from right M1 to right putamen; Figure 2d). Thus, ipsilateral projection is “normally dominant,” and contralateral projection is “normally nondominant”. The labeled pixels above the threshold of the putamen are shown in Figure 2c',d'. The average area above the threshold in the left putamen was 12.1%, while it was 52.9% in the right putamen ($n = 12$, Figure 2g, left). Thus, the ratio of normally nondominant versus normally dominant projections was 0.23 from the unaffected M1. The projections from the contralesional (left; affected) M1 to the putamen are shown in Figure 2b,e,f. The average percentage of labeled pixels in a total of 12 sections spanning from the anterior to posterior portions of the putamen was 55.3% in the left putamen (Figure 2e') and 29.5% (Figure 2f',g, right) in the right putamen. Thus, the ratio of normally nondominant versus normally dominant projections was 0.53 from the affected M1. Therefore, the ratio

of normally nondominant versus normally dominant projections was approximately 2.3 times higher ($t(17) = 6.57$, $p = 0.0000048$, unpaired two-tailed *t*-test) from the affected M1 than from the unaffected M1 (Figure 2g,h). These results suggested that the normally nondominant (contralateral) projection from the contralesional (affected) M1 was increased compared with those from the ipsilesional (unaffected) M1. Here, the corticofugal fibers from the contralesional M1 were labeled with GFP and those from the ipsilesional M1 were labeled with DsRed2, and the staining of the former appeared to be much more intense than that of the latter. One may suspect that such a difference in the intensity of staining might have caused the difference in the ratio of normally nondominant to normally dominant projections described above.

To exclude such a possibility, we switched the side of injection of each viral tracer in the second monkey (Monkey H; AAV-DsRed2 into the contralesional M1 and AAV-GFP into the ipsilesional M1). The results for Monkey H are shown in Figure 2i,j. For the projections from the ipsilesional (right; unaffected) M1, the percentage of labeled pixels in the left putamen averaged 10.5%, while it averaged 41.8% in the right putamen in a total of 13 sections spanning from the anterior to posterior portions of the putamen (Figure 2i). Thus, the ratio of normally nondominant versus normally dominant projections averaged 0.25 from the unaffected M1 (Figure 2j). Conversely, for the projections from the contralesional (left; affected) M1, the averaged percentage of labeled pixels in the left and right putamen was 43.6% and 17.6%, respectively ($n = 13$). Thus, the ratio of normally nondominant versus normally dominant projections was 0.41 from the affected M1 (Figures 2i,j). Here again, the ratio of normally nondominant versus normally dominant projections was approximately 1.6 times higher ($t(19) = 2.32$, $p = 0.032$, unpaired two-tailed *t*-test) from the affected M1 than from the unaffected M1. Although several sections showed a lower ratio of normally nondominant

versus normally dominant projections from the affected M1 than from the unaffected M1, the caudal two-thirds of sections, which were considered to be the main target region from the hand representation area of M1 (Takada et al. 1998), constantly

showed a higher ratio. Thus, the relative increase of normally nondominant (contralateral) projections from the affected M1 compared with that from the unaffected M1 was also consistent in Monkey H.

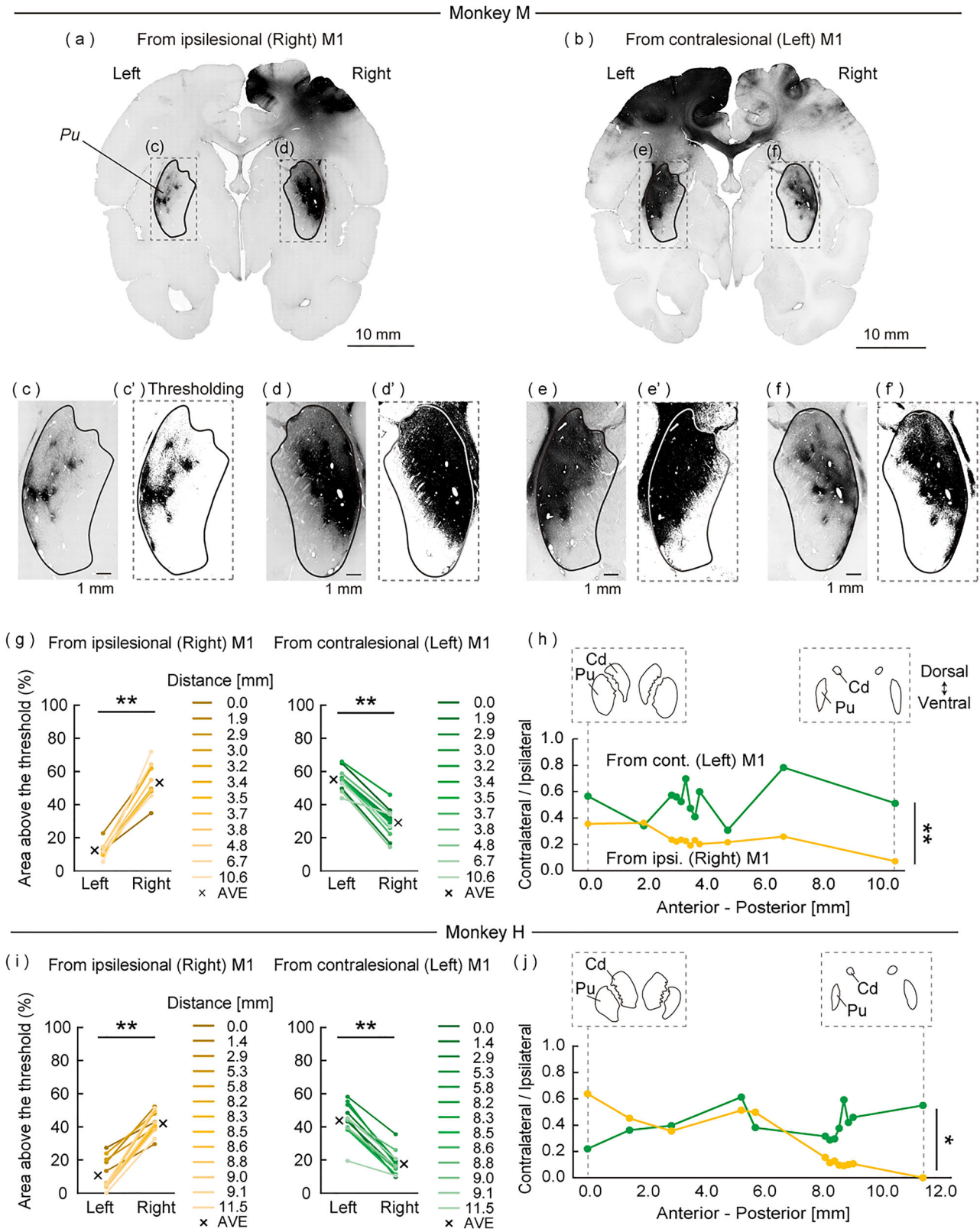


FIGURE 2 | Legend on next page.

3.2 | Projections From the Motor Cortex to the LRN

The projections from the ipsilesional (right; unaffected) M1 to the LRN of Monkey M are shown in Figure 3a. The labeled axons were mainly detected in the left LRN (Figure 3c,g) rather than in the right LRN (Figure 3d,h). Thus, contralateral projections are “normally dominant,” and ipsilateral projections are “normally nondominant” projections. The averaged percentage of labeled pixels in the left LRN (contralateral projections) was 3.26%, whereas it was 1.05% in the right LRN (ipsilateral projections; $n = 9$ sections separated by 0.16 mm from the anterior to the posterior portion of the LRN, Figure 3k). The projections from the contralesional (left; affected) M1 to LRN are shown in Figure 3b. As can be seen in the high magnification images, the density of normally nondominant projections (from left M1 to left LRN; Figure 3e,i) was equal to or even greater than the density of normally dominant projections (from left M1 to right LRN; Figure 3f,j). The averaged percentage of labeled pixels was 52.0% in the left LRN (ipsilateral projections) and 32.1% in the right LRN (contralateral projections; $n = 9$).

The data from these nine sections from the anterior to posterior portion of the LRN are plotted in Figure 3l. For the projections from the unaffected M1, the ratio between the normally nondominant versus normally dominant projections was 0.30–0.97 (average 0.41), while it was 0.85–3.01 (average 1.75) for the projections from the affected M1 ($t(10) = 5.91$, $p = 0.00015$, unpaired two-tailed t -test).

The results for Monkey H are shown in Figure 3m,n. For the projections from ipsilesional (right; unaffected) M1, the percentage of labeled pixels in the left LRN averaged 8.75%, while it averaged 1.97% in the right LRN ($n = 6$; each separated by 0.16 mm). For the projections from the contralesional (left; affected) M1, the averaged percentage of labeled pixels in the left and right LRN was 4.82% and 7.36%, respectively ($n = 6$). Thus, the ratio of normally nondominant versus normally dominant projections was 0.47–0.92 (average 0.68) from the affected M1, whereas it was 0.18–0.43 (average 0.26) from the unaffected M1 ($t(7) = 4.94$, $p = 0.0017$, unpaired two-tailed t -test). Thus, the increase of normally nondominant (ipsilateral) projections to the LRN from the affected M1 compared with that from the unaffected M1 was commonly observed in both monkeys.

3.3 | Projections From the Motor Cortex to the Pontine Nucleus

The projections from the ipsilesional (right; unaffected) M1 to the pontine nucleus in Monkey M are shown in Figure 4a. As

can be seen in the high-magnification images, the labeled axons were detected in the mediodorsal part of the right pontine nucleus (Figure 4d), but there were almost none in the corresponding region of the left pontine nucleus (Figure 4c). Here, the ipsilateral projections are “normally dominant” and contralateral projections are “normally nondominant” projections. The averaged percentage of labeled pixels originating from the ipsilesional (right; unaffected) M1 was 1.56% in the left pontine nucleus and 43.2% in the right pontine nucleus ($n = 6$ sections separated by 0.48 mm from the rostral to caudal end of the pontine nucleus, Figure 4g). That is, the ratio of normally nondominant versus normally dominant projections was 0.036 from the ipsilesional M1. In contrast, for the projections from the contralesional (left; affected) M1, the labeled axons were detected on both sides of the pontine nucleus (Figure 4b,e,f). The averaged percentage of labeled pixels originating from the contralesional (left; affected) M1 was 68.3% in the left pontine nucleus and 21.4% in the right pontine nucleus. That is, the ratio of normally nondominant versus normally dominant projections was 0.31 from the contralesional (left) M1 ($n = 6$, Figure 4g). These results indicate that the ratio of normally nondominant versus normally dominant projections was 8.8 times higher from the affected M1 than from the unaffected M1 ($t(6) = 6.60$, $p = 0.00058$, unpaired two-tailed t -test, Figure 4h).

In Monkey H, the percentages of labeled pixels in the corresponding regions of the pontine nucleus on the left and right sides were 0.51% and 8.48%, respectively (Figure 4i, left and Figure 4j, orange), for the projections from the ipsilesional (right; unaffected) M1 ($n = 6$ sections separated by 0.48 mm from the rostral to caudal end of the pontine nucleus). That is, the ratio of normally nondominant versus normally dominant projections was 0.061 from the ipsilesional M1. In contrast, for the projections from the contralesional (left, affected) M1, the percentage of labeled pixels was 16.1% in the left pontine nucleus and 3.61% in the right pontine nucleus ($n = 6$; Figure 4i, right and Figure 4j, green). That is, the ratio of normally nondominant versus normally dominant projections was 0.23 from the contralesional M1. These results indicate that the ratio of normally nondominant versus normally dominant projections was also increased for the projections from the affected M1 in Monkey H ($t(6) = 2.69$, $p = 0.036$, unpaired two-tailed t -test).

4 | Discussion

Most of the previous research on the neural mechanisms of recovery after spinal cord injury has focused on either how to reconnect the damaged nerve tract by removing the glial scars that prevent the regeneration of nerve fibers (Hollis et al.

FIGURE 2 | Projections from the primary motor cortex (M1) to the putamen (Pu). (a–f) Immunohistochemical staining of coronal brain sections detecting the corticofugal fibers originating from the ipsilesional M1 (a, c, d; anti-DsRed2 antibody) and contralesional M1 (b, e, f; anti-GFP antibody) in Monkey M. c'–f' are thresholding binary images of c–f. (g) Percentage of pixels with signal intensity above the threshold in the left and right Pu for the projections from the ipsilesional (right) M1 (left graph) and contralesional (left) M1 (right graph). Values obtained in the same sections are connected (see the corresponding colors in the inset) and their average values are indicated by crosses. $**p < 0.01$, paired two-tailed t -test. (h) Proportion of contralateral projections to the Pu versus ipsilateral projections originating from the ipsilesional M1 (orange) and contralesional M1 (green) in 12 sections from anterior to posterior. Illustrations of the striatum shown in the dotted squares indicate its structure in the most anterior (0.00 mm) and most posterior (10.6 mm) sections. $**p < 0.01$, unpaired two-tailed t -test. (i, j) Data in the same format as in g and h, but from Monkey H. $*p < 0.05$; $**p < 0.01$ ($n = 13$). AVE, average; Cd, caudate; cont., contralesional; ipsi., ipsilesional.

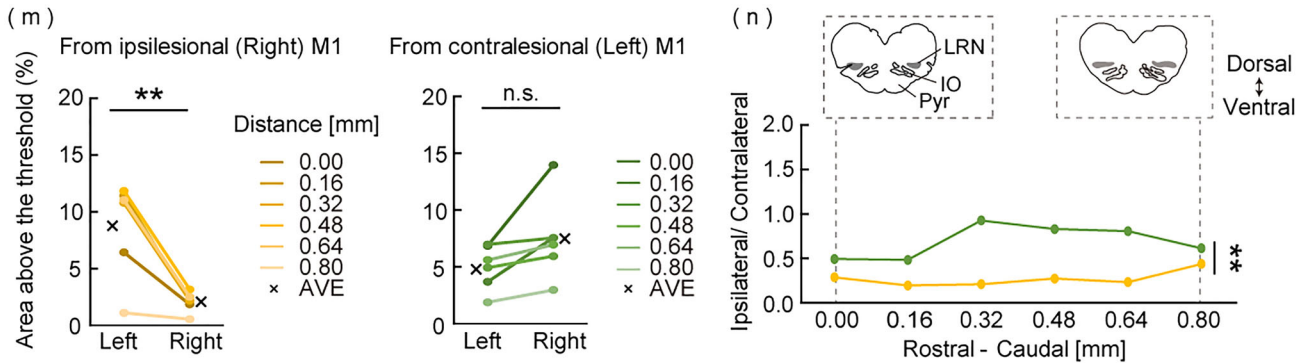
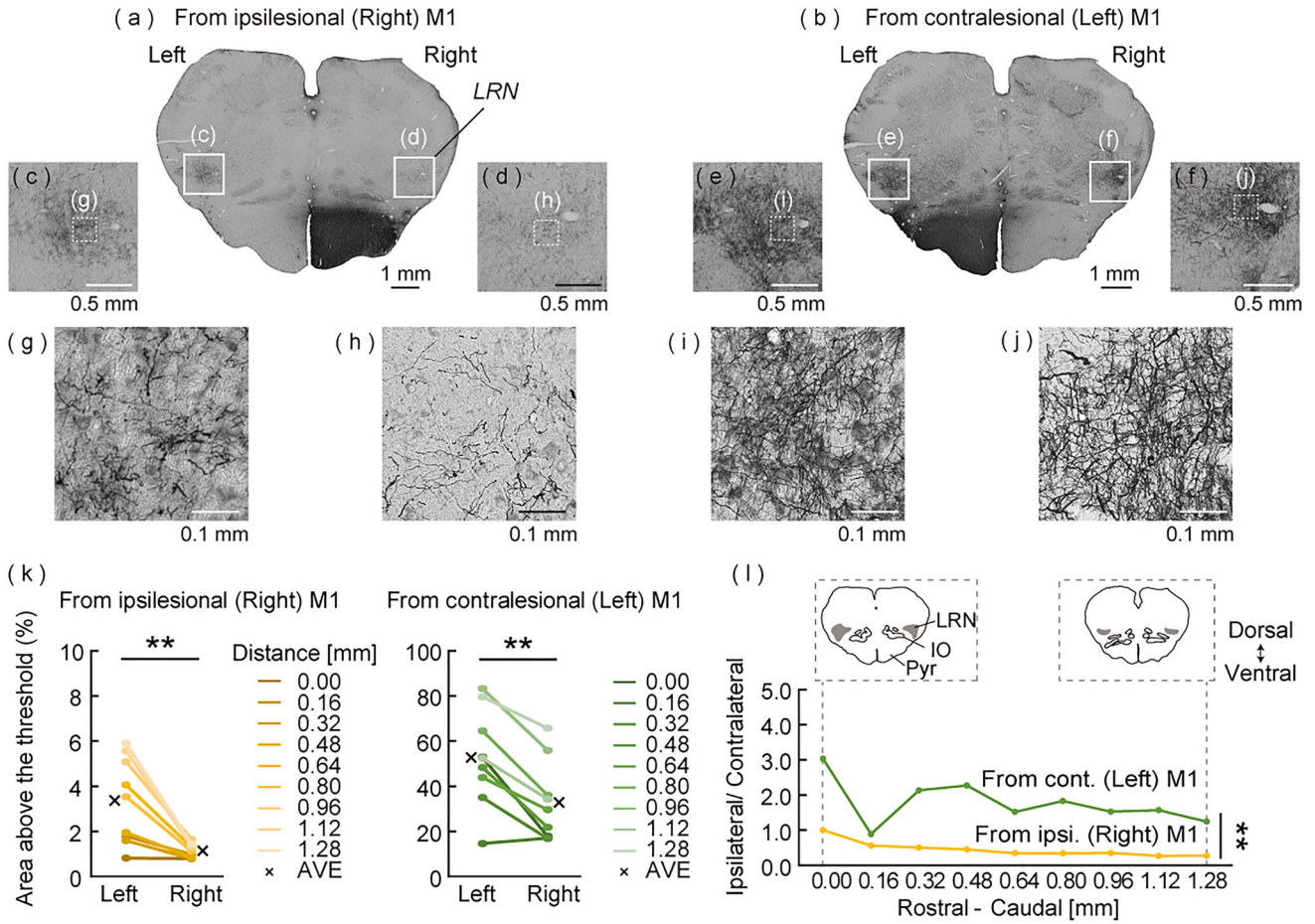


FIGURE 3 | Projections from the primary motor cortex (M1) to the LRN. (a–j) Immunohistochemical staining of coronal sections of the medulla oblongata detecting the corticofugal fibers originating from the ipsilesional M1 (a, c, d, g, h; anti-DsRed2 antibody) and contralesional M1 (b, e, f, i, j; anti-GFP antibody) in Monkey M. The locations of c and d are indicated as in a and the locations of g and h are indicated with dotted squares in c and d. Similar arrangements for b, e, f, i, and j. (k) Percentage of pixels with signal intensity above the threshold in the left and right LRN for the projections from the ipsilesional (right) M1 (left graph) and contralesional (left) M1 (right graph). Values obtained in the same sections are connected (see the corresponding colors in the inset) and their average values are indicated by crosses. $**p < 0.01$, paired two-tailed *t*-test. (l) Proportion of ipsilateral projections to the LRN versus contralateral projections originating from the ipsilesional M1 (orange) and contralesional M1 (green) in nine sections separated by 0.16 mm from rostral to caudal. Illustrations shown in the dotted square indicate the brainstem structure in the most anterior (0.00 mm) and most posterior (1.28 mm) sections of the analyzed sections. $**p < 0.01$, unpaired two-tailed *t*-test. (m, n) Data in the same format as in k and l, but from Monkey H. $n.s. p \geq 0.05$; $**p < 0.01$ ($n = 6$). AVE, average; cont., contralesional; IO, inferior olive; ipsi., ipsilesional; Pyr, pyramid.

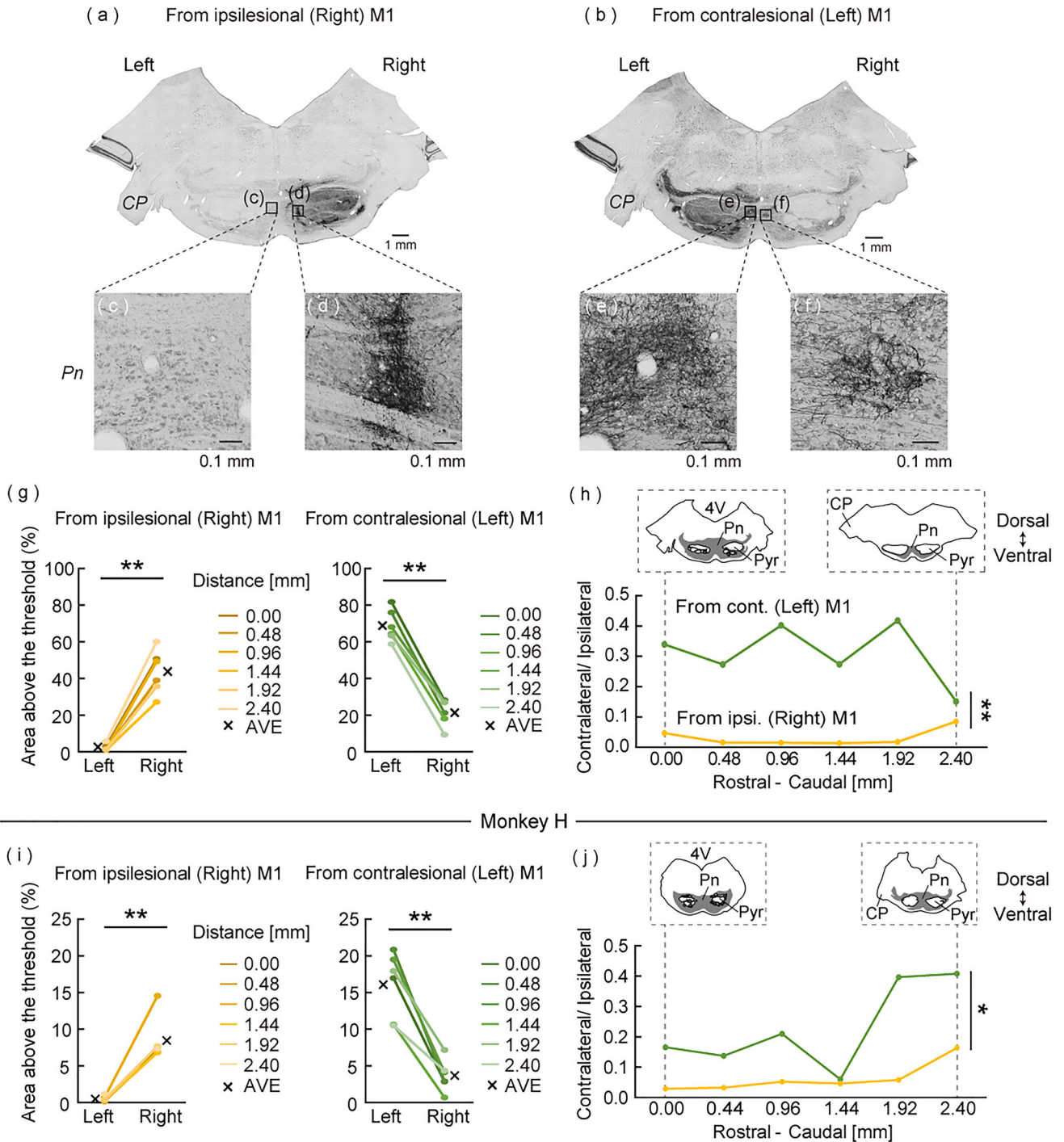


FIGURE 4 | Projections from the primary motor cortex (M1) to the pontine nucleus (Pn). (a–f) Immunohistochemical staining of coronal sections of the pons detecting the corticofugal fibers originating from the ipsilesional M1 (a, c, d; anti-DsRed2 antibody) and contralesional M1 (b, e, f; anti-GFP antibody) in Monkey M. The locations of c and d are indicated as squares in a and the locations of e and f are indicated with squares in b. (g) Percentage of pixels with signal intensity above the threshold in the left and right Pn. Values obtained in the same sections are connected (see the corresponding colors in the inset) and their average values are indicated by crosses. $**p < 0.01$, paired two-tailed *t*-test. (h) Proportion of contralateral projections versus ipsilateral projections to the Pn originating from the ipsilesional M1 (orange) and contralesional M1 (green) in six sections separated by 0.48 mm from rostral to caudal. Illustrations shown in dashed indicate the brainstem structure at the most anterior (0.00 mm) and most posterior (2.40 mm) sections of the analyzed sections. $**p < 0.01$, unpaired two-tailed *t*-test. (i, j) Data in the same format as in g and h from Monkey H. $*p < 0.05$; $**p < 0.01$ ($n = 6$). 4V, fourth ventricle; AVE, average; CP, cerebral peduncle; Pyr, pyramid.

2016; Ueno et al. 2020; Wang et al. 2020) or how to promote the remaining neural systems to take over the functions of the damaged circuits by inducing neural plasticity (Raineteau and Schwab 2001). These studies have targeted how to recover the connection from the brain to motoneurons (Tohyama et al. 2017) or how to reconnect the sensory input to the brain (Moreno-López and Hollis 2021).

Our group has been studying the plasticity of the descending motor pathways from the contralesional (affected) or ipsilesional (unaffected) M1 after partial spinal cord injury in macaque monkeys (Isa 2017; Isa, Mitsuhashi, and Yamaguchi 2019; Sawada et al. 2023). Particularly, in a subhemisection injury model (Yamaguchi et al. 2023), the animals did not recover precision grip, but upon the administration of extensive cortical electrical stimulation, they showed quick recovery of coarse hand movements, which were not observed in animals without stimulation. These animals showed massive plasticity of the corticospinal tract below the pyramidal decussation.

In the present study, we analyzed the trajectories of corticofugal fibers at the supraspinal level and interestingly, found an increased number of projections of corticofugal fibers originating from the affected (contralesional) M1 to the putamen and precerebellar brain stem nuclei such as the LRN and pontine nucleus on the nondominant side (Table 1).

The effect of cortical stimulation and behavioral training on the plastic changes of the corticofugal fibers observed in this study is a highly significant issue that needs to be clarified. Because previous studies have shown similar lesion results in slow and limited spontaneous recovery (Galea and Darian-Smith 1997; Rosenzweig et al. 2010; Nakagawa et al. 2015), we expect that the plastic changes of axonal trajectories observed in this study are unlikely to occur without additional treatments. However, to confirm this, a number of additional control experiments will be needed involving a certain number of animals with either behavioral training or cortical stimulation alone following the subhemisection injury for future studies. Below, we discuss how to interpret the present findings.

4.1 | Functional Significance of Plasticity in the Cortico-Striatal Projections

It is known that the cortico-striatal pathway comprises a part of the cortico-basal ganglia loops. It is generally considered that the cortico-basal ganglia loops consist of the direct pathway (cortex—striatum—internal segment of the globus pallidus or substantia nigra pars reticulata—thalamus—cortex) and indirect pathway (cortex—striatum—external segment of the globus pallidus—subthalamus—internal segment of the globus pallidus or substantia nigra pars reticulata—thalamus—cortex) and are involved in motor planning (yellow in Figure 5a; here, only the direct pathway is illustrated). In the cortico-striatal pathway, the ipsilateral projections dominate the contralateral projections, but there are also less dominant cortical projections to the contralateral striatum (Künzle 1975). However, the function of the contralateral cortico-striatal projections is unclear. In addition to the previously reported massive re-routing below the spinal decussation (Yamaguchi et al. 2023), here we found that the corti-

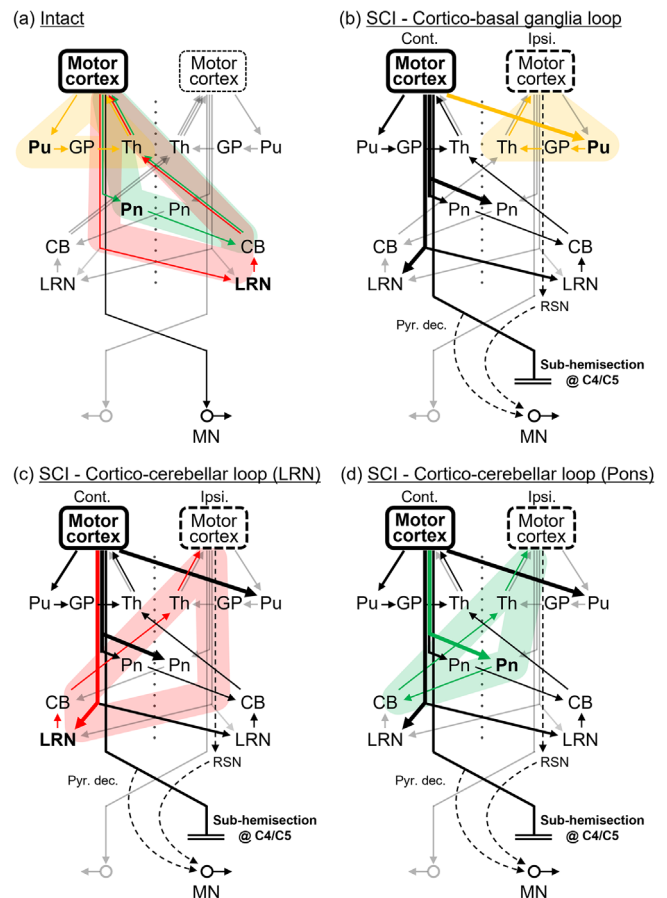


FIGURE 5 | Schematic illustration of the critical neural circuits in the intact case (a) and spinal cord injury (SCI) case (b–d). Cortico-basal ganglia loop through the putamen (Pu) and cortico-cerebellar loops through the LRN and pontine nucleus (Pn) are highlighted with yellow, red, and green, respectively. The target regions of this study are indicated in bold letters. The neural pathways in question are indicated in bold lines. CB, cerebellum; Cont., contralesional side; GP, Globus Pallidus; Ipsi., ipsilesional side; MN, motoneurons; Pyr. dec., pyramidal decussation; RSN, reticulospinal neurons; Th, thalamus.

cofugal fibers from the affected M1 increased their projections to the contralateral putamen during recovery from subhemisection spinal cord injury (Figure 2). They were mainly targeted to the dorsolateral part of the contralateral putamen, which was a mirror image of the normal projections to the ipsilateral putamen. This means that neurons in the labeled area in the ipsilesional putamen increased the amount of input from the contralesional M1 in addition to the ipsilesional M1. This observation suggests that the target area in the ipsilesional putamen has a functional linkage with the ipsilesional M1 through the cortico-basal ganglia loop on the ipsilesional side. In Monkeys M and H, we have found increased activity in the ipsilesional M1 during recovery (Yamaguchi et al. 2023). Therefore, we propose a hypothesis that the increased projections from the contralesional M1 to the ipsilesional putamen may function for the contralesional M1 to increase the activity of ipsilesional M1 through the cortico-basal ganglia loop and recruit it into movement control together with the cortico-basal ganglia loop on the contralesional side (Figure 5b).

4.2 | Functional Significance of Plasticity in the Pre-Cerebellar Nuclei

The LRN and pontine nucleus project to the cerebellum and comprise a part of the cortico-cerebellar loop (Gao et al. 2018). The LRN receives input from the contralateral motor cortex and sends input to the ipsilateral cerebellum via the inferior cerebellar peduncle (Figure 5a, red). The pontine nucleus receives input mainly from the ipsilateral motor cortex and sends input to the contralateral cerebellum via the middle cerebellar peduncle (Figure 5a, green). Then, the output from the cerebellum regulates movements through indirect connections to the contralateral motor cortex via the ventral lateral nucleus of the thalamus (or more directly through projections to the contralateral red nucleus and rubrospinal tract) (Na, Kakei, and Shinoda 1997). Thus, the increased projections from the affected M1 to the contralateral side of the normally dominant side (the contralesional LRN and ipsilesional pontine nucleus) would function for the contralesional M1 to activate the ipsilesional (unaffected) M1 through the cortico-cerebellar loop on the contralateral side (Figure 5c,d). Since the cortico-cerebellar loops are supposed to play critical roles in motor planning (Gao et al. 2018), we wish to propose a hypothesis that they may contribute to the recovery of hand movements through the activation of the ipsilesional M1 after spinal cord injury.

4.3 | Cell Types Underlying the Plastic Changes

Previous studies, mainly on rodents, revealed that corticostriatal and corticopontine projections originate from different cortical cell types (Morishima and Kawaguchi 2006; Shepherd 2013). The former projections originate from an “intratelencephalic neuron” cell type, from which the cortico-cortical and corticostriatal projections originate. The latter projections originate from a “pyramidal neuron” cell type, from which the cortico-pontine, cortico-medullary, and corticospinal projections originate. The present findings demonstrated that both cell types increased their axonal projections to the putamen, LRN, and pontine nucleus contralateral to the dominant target. They receive different inputs (Garcia et al. 2021) and behave differently in motor control (Nambu 2008; Park et al. 2022). How their plasticity is coordinated would be a future target of research on functional recovery after spinal cord injury.

4.4 | Involvement of the Ipsilesional Sensorimotor Cortex in Recovery After Spinal Cord Injury

Our previous study showed that Granger causality from the contralesional motor cortex to the ipsilesional motor cortex is enhanced during recovery from spinal cord injury (Chao et al. 2019). How could the contralesional motor cortex activate the ipsilesional motor cortex? There are two possible pathways: the cortico-cortical (callosal) or cortico-subcortical pathway (either through the basal ganglia or cerebellum or both).

Our recent study showed that the ipsilesional motor cortex is activated by the callosal pathway from the contralesional premotor cortex during recovery from spinal cord injury, mainly at the low-frequency band (7–9 Hz) (Mitsuhashi et al. 2024). This

result suggests that the callosal input from the contralesional premotor cortex does not send high- γ band activity directly to the ipsilesional M1, which is critical for the control of hand movements on the ipsilesional side (Chao et al. 2019).

Thus, there is a possibility that the low-frequency band component is conveyed directly through the callosal fibers and plays a role in gating the motor commands in the M1, while the high-frequency band component is transmitted to the M1 through separate systems, such as the cortico-basal ganglia or cortico-cerebellar loops. Here, we propose that for functional recovery after spinal cord injury, if the neural system starts to recruit the ipsilesional M1, which is not primarily involved in motor control before injury, reconnection from the brain to motoneurons alone may not be enough. The results of this study support the hypothesis that higher-order control systems, such as the cortico-basal ganglia or cortico-cerebellar loops, should be recruited for the more efficient control of movement. To prove this hypothesis, further studies are needed to investigate the effects of perturbing transmission through the cortico-basal ganglia and/or cortico-cerebellar loops during recovery from spinal cord injury.

Author Contributions

Satoko Ueno, Kaoru Isa and Tadashi Isa designed all the details of anatomical experiments with support from Jun Takahashi regarding precise localization of tracer injections with MRI. Kenta Kobayashi designed and produced the viral tools. Reona Yamaguchi, Toshinari Kawasaki, Masahiro Mitsuhashi, Satoko Ueno, and Tadashi Isa designed and performed the surgeries of spinal cord injury and tracer injections. Reona Yamaguchi, Toshinari Kawasaki, Masahiro Mitsuhashi, and Satoko Ueno conducted behavioral training and recordings before and after the spinal cord injury. Satoko Ueno and Kaoru Isa conducted the histological experiments and analyzed the histological data. Satoko Ueno and Tadashi Isa wrote the manuscript with inputs from all the authors.

Acknowledgments

We are grateful to Kei Kubota for technical assistance. This work was supported by a Grant-in-Aid for Scientific Research on Innovative Areas “Hyper-adaptability” to T.I. (Project no. 19H05723), a Grant-in-Aid for Scientific Research from the Ministry of Education, Culture, Sports, Science, and Technology (MEXT) to T.I. (KAKENHI (A) no. 19H01011 and (S) no. 22H04992), Japan Agency for Medical Research and Development (JP18dm0307005 to T.I.), and a Grant-in-Aid for Research Activity Start-up to S.U. (Project no. 22K21240).

Conflicts of Interest

The authors declare no conflicts of interest.

Data Availability Statement

The data that support the findings of this study are available from the corresponding author upon reasonable request.

Peer Review

The peer review history for this article is available at <https://publons.com/publon/10.1002/cne.70007>.

References

- Alexander, G. E., M. R. DeLong, and P. L. Strick. 1986. "Parallel Organization of Functionally Segregated Circuits Linking Basal Ganglia and Cortex." *Annual Review of Neuroscience* 9: 357–381. <https://doi.org/10.1146/annurev.ne.09.030186.002041>.
- Alstermark, B., and T. Isa. 2012. "Circuits for Skilled Reaching and Grasping." *Annual Review of Neuroscience* 35: 559–578. <https://doi.org/10.1146/annurev-neuro-062111-150527>.
- Chao, Z. C., M. Sawada, T. Isa, and Y. Nishimura. 2019. "Dynamic Reorganization of Motor Networks during Recovery From Partial Spinal Cord Injury in Monkeys." *Cerebral Cortex* 29, no. 7: 3059–3073. <https://doi.org/10.1093/cercor/bhy172>.
- Courtine, G., M. B. Bunge, J. W. Fawcett, et al. 2007. "Can Experiments in Nonhuman Primates Expedite the Translation of Treatments for Spinal Cord Injury in Humans?" *Nature Medicine* 13, no. 5: 561–566. <https://doi.org/10.1038/nm1595>.
- Darian-Smith, C. 2007. "Monkey Models of Recovery of Voluntary Hand Movement After Spinal Cord and Dorsal Root Injury." *ILAR Journal* 48, no. 4: 396–410. <https://doi.org/10.1093/ilar.48.4.396>.
- Galea, M. P., and I. Darian-Smith. 1997. "Manual Dexterity and Corticospinal Connectivity Following Unilateral Section of the Cervical Spinal Cord in the Macaque Monkey." *Journal of Comparative Neurology* 381, no. 3: 307–319.
- Gao, Z., C. Davis, A. M. Thomas, et al. 2018. "A Cortico-Cerebellar Loop for Motor Planning." *Nature* 563, no. 7729: 113–116. <https://doi.org/10.1038/s41586-018-0633-x>.
- Garcia, A. F., E. A. Crummy, I. G. Webb, M. N. Nooney, and S. M. Ferguson. 2021. "Distinct Populations of Cortical Pyramidal Neurons Mediate Drug Reward and Aversion." *Nature Communications* 12, no. 1: 182. <https://doi.org/10.1038/s41467-020-20526-0>.
- Guillery, R. W., and S. M. Sherman. 2002. "The Thalamus as a Monitor of Motor Outputs." *Philosophical Transactions of the Royal Society of London. Series B, Biological Sciences* 357, no. 1428: 1809–1821. <https://doi.org/10.1098/rstb.2002.1171>.
- Hollis, E. R., II, N. Ishiko, T. Yu, et al. 2016. "Ryk Controls Remapping of Motor Cortex During Functional Recovery After Spinal Cord Injury." *Nature Neuroscience* 19, no. 5: 697–705. <https://doi.org/10.1038/nn.4282>.
- Isa, T. 2017. "The Brain Is Needed to Cure Spinal Cord Injury." *Trends in Neurosciences* 40, no. 10: 625–636. <https://doi.org/10.1016/j.tins.2017.08.002>.
- Isa, T., M. Mitsuhashi, and R. Yamaguchi. 2019. "Alternative Routes for Recovery of Hand Functions After Corticospinal Tract Injury in Primates and Rodents." *Current Opinion in Neurology* 32, no. 6: 836–843. <https://doi.org/10.1097/WCO.0000000000000749>.
- Jankowska, E., K. Stecina, A. Cabaj, L. G. Pettersson, and S. A. Edgley. 2006. "Neuronal Relays in Double Crossed Pathways Between Feline Motor Cortex and Ipsilateral Hindlimb Motoneurons." *Journal of Physiology* 575, no. Pt 2: 527–541. <https://doi.org/10.1113/jphysiol.2006.112425>.
- Künzle, H. 1975. "Bilateral Projections From Precentral Motor Cortex to the Putamen and Other Parts of the Basal Ganglia. An Autoradiographic Study in *Macaca fascicularis*." *Brain Research* 88, no. 2: 195–209. [https://doi.org/10.1016/0006-8993\(75\)90384-4](https://doi.org/10.1016/0006-8993(75)90384-4).
- Lemon, R. N. 2008. "Descending Pathways in Motor Control." *Annual Review of Neuroscience* 31: 195–218. <https://doi.org/10.1146/annurev.neuro.31.060407.125547>.
- Mitsuhashi, M., R. Yamaguchi, T. Kawasaki, et al. 2024. "Stage-Dependent Role of Interhemispheric Pathway for Motor Recovery in Primates." *Nature Communications* 15, no. 1: 6762. <https://doi.org/10.1038/s41467-024-51070-w>.
- Moreno-López, Y., and E. R. Hollis. 2021. "Sensory Circuit Remodeling and Movement Recovery after Spinal Cord Injury." *Frontiers in Neuroscience* 15: 787690. <https://doi.org/10.3389/fnins.2021.787690>.
- Morishima, M., and Y. Kawaguchi. 2006. "Recurrent Connection Patterns of Corticostriatal Pyramidal Cells in Frontal Cortex." *Journal of Neuroscience* 26, no. 16: 4394–4405. <https://doi.org/10.1523/JNEUROSCI.0252-06.2006>.
- Na, J., S. Kakei, and Y. Shinoda. 1997. "Cerebellar Input to Corticothalamic Neurons in Layers V and VI in the Motor Cortex." *Neuroscience Research* 28, no. 1: 77–91. [https://doi.org/10.1016/s0168-0102\(97\)00031-x](https://doi.org/10.1016/s0168-0102(97)00031-x).
- Nakagawa, H., T. Ninomiya, T. Yamashita, and M. Takada. 2015. "Reorganization of Corticospinal Tract Fibers After Spinal Cord Injury in Adult Macaques." *Scientific Reports* 5: 11986. <https://doi.org/10.1038/srep11986>.
- Nambu, A. 2008. "Seven Problems on the Basal Ganglia." *Current Opinion in Neurobiology* 18, no. 6: 595–604. <https://doi.org/10.1016/j.conb.2008.11.001>.
- Nishimura, Y., H. Onoe, Y. Morichika, S. Perfiliev, H. Tsukada, and T. Isa. 2007. "Time-Dependent Central Compensatory Mechanisms of Finger Dexterity After Spinal Cord Injury." *Science* 318, no. 5853: 1150–1155. <https://doi.org/10.1126/science.1147243>.
- Park, J., J. W. Phillips, J. Z. Guo, K. A. Martin, A. W. Hantman, and J. T. Dudman. 2022. "Motor Cortical Output for Skilled Forelimb Movement Is Selectively Distributed Across Projection Neuron Classes." *Science Advances* 8, no. 10: eabj5167. <https://doi.org/10.1126/sciadv.abj5167>.
- Raineteau, O., and M. E. Schwab. 2001. "Plasticity of Motor Systems After Incomplete Spinal Cord Injury." *Nature Reviews Neuroscience* 2, no. 4: 263–273. <https://doi.org/10.1038/35067570>.
- Rosenzweig, E. S., G. Courtine, D. L. Jindrich, et al. 2010. "Extensive Spontaneous Plasticity of Corticospinal Projections After Primate Spinal Cord Injury." *Nature Neuroscience* 13, no. 12: 1505–1510. <https://doi.org/10.1038/nn.2691>.
- Sano, H., K. Kobayashi, N. Yoshioka, H. Takebayashi, and A. Nambu. 2020. "Retrograde Gene Transfer Into Neural Pathways Mediated by Adeno-Associated Virus (AAV)-AAV Receptor Interaction." *Journal of Neuroscience Methods* 345: 108887. <https://doi.org/10.1016/j.jneumeth.2020.108887>.
- Sasaki, S., T. Isa, L. G. Pettersson, et al. 2004. "Dexterous Finger Movements in Primate Without Monosynaptic Corticomotoneuronal Excitation." *Journal of Neurophysiology* 92, no. 5: 3142–3147. <https://doi.org/10.1152/jn.00342.2004>.
- Sawada, M., K. Yoshino-Saito, T. Ninomiya, et al. 2023. "Reorganization of Corticospinal Projections After Prominent Recovery of Finger Dexterity From Partial Spinal Cord Injury in Macaque Monkeys." *Eneuro* 10, no. 8: ENEURO.0209–0223.2023. <https://doi.org/10.1523/ENEURO.0209-23.2023>.
- Shepherd, G. M. 2013. "Corticostriatal Connectivity and Its Role in Disease." *Nature Reviews Neuroscience* 14, no. 4: 278–291. <https://doi.org/10.1038/nrn3469>.
- Sugiyama, Y., N. Higo, K. Yoshino-Saito, et al. 2013. "Effects of Early Versus Late Rehabilitative Training on Manual Dexterity After Corticospinal Tract Lesion in Macaque Monkeys." *Journal of Neurophysiology* 109, no. 12: 2853–2865. <https://doi.org/10.1152/jn.00814.2012>.
- Takada, M., H. Tokuno, A. Nambu, and M. Inase. 1998. "Corticostriatal Projections From the Somatic Motor Areas of the Frontal Cortex in the Macaque Monkey: Segregation Versus Overlap of Input Zones From the Primary Motor Cortex, the Supplementary Motor Area, and the Premotor Cortex." *Experimental Brain Research* 120, no. 1: 114–128. <https://doi.org/10.1007/s002210050384>.
- Tohyama, T., M. Kinoshita, K. Kobayashi, et al. 2017. "Contribution of Proprioceptive Neurons to Recovery of Hand Dexterity After Corticospinal Tract Lesions in Monkeys." *Proceedings of the National Academy of Sciences of the United States of America* 114, no. 3: 604–609. <https://doi.org/10.1073/pnas.1610787114>.
- Ueno, M., Y. Nakamura, H. Nakagawa, et al. 2020. "Olig2-Induced Semaphorin Expression Drives Corticospinal Axon Retraction After Spinal Cord Injury." *Cerebral Cortex* 30, no. 11: 5702–5716. <https://doi.org/10.1093/cercor/bhaa142>.

Wang, X., T. Zhou, G. D. Maynard, et al. 2020. “Nogo Receptor Decoy Promotes Recovery and Corticospinal Growth in Non-Human Primate Spinal Cord Injury.” *Brain* 143, no. 6: 1697–1713. <https://doi.org/10.1093/brain/awaa116>.

Yamaguchi, R., S. Ueno, T. Kawasaki, et al. 2023. “Global Disinhibition and Massive Corticospinal Plasticity for Drastic Recovery After Spinal Cord Injury.” *bioRxiv*. <https://doi.org/10.1101/2023.03.15.532773>.